

Pinning down anomalous $WW\gamma$ couplings at the LHC

Disha Bhatia,^{*} Ushoshi Maitra,[†] and Sreerup Raychaudhuri[‡]

*Department of Theoretical Physics, Tata Institute of Fundamental Research,
1 Homi Bhabha Road, Mumbai 400 005, India*

 (Received 22 May 2018; revised manuscript received 23 October 2018; published 16 May 2019)

We make a careful analysis of $W^\pm\gamma$ production at the LHC, identifying the W^\pm through leptonic decays, with a view to exploring the sensitivity of the machine to anomalous CP -conserving $WW\gamma$ interactions. All the available kinematic variables are used, but we find that the most useful one is the opening angle in the transverse plane between the decay products of the W^\pm . It is shown that even a simple-minded analysis using this variable can lead to a much greater sensitivity at the LHC than the current constraints on the relevant parameters.

DOI: [10.1103/PhysRevD.99.095017](https://doi.org/10.1103/PhysRevD.99.095017)

The initial euphoria over the Higgs boson discovery of 2012 [1] has now more or less abated, and even after more than a year's running of the CERN Large Hadron Collider (LHC) at the upgraded energy of 13 TeV, there have been no signs of new physics beyond the Standard Model (SM) [2]. However, while it has become abundantly clear that the belief that new particles and interactions would be discovered as soon as the LHC upgrade began to run was overly optimistic, there is no reason for despondency—as yet [3]. This is because most of the new physics models proposed are of the decoupling type, with (possibly) highly massive particles and very feeble interactions, and may therefore prove much more difficult to discover than we have hitherto imagined—or hoped. At this juncture, we may quickly fortify ourselves by noting that the last serendipitous discovery of an elementary particle (the τ -lepton) occurred more than 40 years ago, and that both the Higgs boson and the phenomena of neutrino oscillations took about the same time or even longer to establish experimentally. It is probably necessary, therefore, for high energy physicists to settle down for a long, hard grind before the expected new physics effects can be observed. For exist they must, if our ideas about quantum field theory, gravitation and cosmology are at all correct [4]. In any case, that a theory with as many *ad hoc* features as the SM can be the ultimate truth about nature is unacceptable to many.

If we assume that there *is* new physics, but it consists of particles too massive to be discovered at the LHC, at least in the early stages of its 13 TeV run, then the only way in which these particles can be observed is through quantum effects, either at the tree or the loop levels. These will appear as modifications to the SM vertices, or the appearance of new, often higher-dimensional, operators involving the SM fields, with coefficients which are rendered small by the heavy mass scale of the underlying physics. Such effective field theories—involving only the field content of the SM—seem to offer the most promising window into physics beyond the SM [5]. However, effective theories have their own problem. Most so-called UV-complete models beyond the Standard Model have only a limited set of operators because of the twin constraints of gauge invariance (or extended gauge symmetries) and renormalizability. In contrast, effective field theories may have a low-lying cutoff, which removes the requirement of renormalizability and permits a proliferation of operators—all with small, but unknown coefficients. With so many unknown parameters, and only a finite set of measurables, almost any phenomenon can, in general, be explained and almost any prediction can be made. This is, if anything, a worse situation than the minimal SM even with all its *ad hoc* features.

It follows from the above that the broad picture of effective field theories is not perhaps the best approach to probe physics beyond the SM. The focus in recent times has been, therefore, on a more minute examination of the operators, and on measurables which depend significantly on only a limited set of these operators, rather than the whole set—an exercise which goes under the misnomer of “simplified models,” for it is the examination rather than the model which is simplified. Perhaps one of the earliest of these focused examinations has been that of *anomalous* triple gauge-boson couplings (TGCs) [6,7], which started

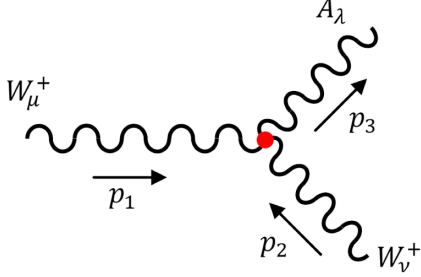
^{*}disha@theory.tifr.res.in

[†]ushoshimaitra32@gmail.com

[‡]sreerup@theory.tifr.res.in

Published by the American Physical Society under the terms of the Creative Commons Attribution 4.0 International license. Further distribution of this work must maintain attribution to the author(s) and the published article's title, journal citation, and DOI. Funded by SCOAP³.

from the days of the LEP collider [8] and have acquired new relevance in the present climate [9–11]. These are anomalous, of course, only in the sense of being absent in the SM at tree level. The TGCs which have been considered are possible modifications to the $W^+W^-\gamma$ and W^+W^-Z vertices, and possible new $ZZ\gamma$, $Z\gamma\gamma$ and ZZZ vertices [12].



This article takes just one of these vertices, viz., the $W^+W^-\gamma$ vertex illustrated on the left and considers a specific final state which is only affected by changes to this vertex. The process in question is

$$p + p \rightarrow W^\pm + \gamma$$

where the $W^\pm \rightarrow \ell^\pm \nu_\ell (\bar{\nu}_\ell)$ for $\ell = e, \mu$ and perhaps τ . The proper bottom-up approach to anomalous vertices in this case is to consider effective higher-dimensional operators which retain the symmetries of the Standard Model, but are suppressed by some high energy scale. At electroweak energies, these will give rise to anomalous TGCs, but these will, in general, be related to the Wilson coefficients of the higher-dimension operators because of the gauge and global symmetries of the Standard Model. Such an approach is advocated in Ref. [13] and is currently being followed by the experimental collaborations [14]. However, our present work has a very limited purpose, and therefore it is easier to compare our results with experiment if we use the older parametrization, assuming that the anomalous TGCs which are not being considered here will fall in line with the symmetries of the theory. Accordingly, if we denote the $W_\mu^+ W_\nu^- A_\lambda$ vertex by $i\Gamma_{\mu\nu\lambda}^{(WW\gamma)}$, then the most general CP -conserving form consistent with the gauge and Lorentz symmetries of the SM can be parametrized [6] in the form of three separate terms, viz.

$$i\Gamma_{\mu\nu\lambda}^{WW\gamma}(p_1, p_2, p_3) = ie \left[T_{\mu\nu\lambda}^{(0)}(p_1, p_2, p_3) + \Delta\kappa_\gamma T_{\mu\nu\lambda}^{(1)}(p_1, p_2, p_3) + \frac{\lambda_\gamma}{M_W^2} T_{\mu\nu\lambda}^{(2)}(p_1, p_2, p_3) \right] \quad (1)$$

where the $T_{\mu\nu\lambda}$ tensors are, respectively,

$$\begin{aligned} T_{\mu\nu\lambda}^{(0)} &= g_{\mu\nu}(p_1 - p_2)_\lambda + g_{\nu\lambda}(p_2 - p_3)_\mu + g_{\lambda\mu}(p_3 - p_1)_\nu \\ T_{\mu\nu\lambda}^{(1)} &= g_{\lambda\mu}p_{3\nu} - g_{\nu\lambda}p_{3\mu} \\ T_{\mu\nu\lambda}^{(2)} &= p_{1\lambda}p_{2\mu}p_{3\nu} - p_{1\nu}p_{2\lambda}p_{3\mu} \\ &\quad - g_{\mu\nu}(p_2 \cdot p_3 p_{1\lambda} - p_3 \cdot p_1 p_{2\lambda}) \\ &\quad - g_{\nu\lambda}(p_3 \cdot p_1 p_{2\mu} - p_1 \cdot p_2 p_{3\mu}) \\ &\quad - g_{\mu\lambda}(p_1 \cdot p_2 p_{3\nu} - p_2 \cdot p_3 p_{1\nu}). \end{aligned} \quad (2)$$

The tensor $T_{\mu\nu\lambda}^{(0)}$ in Eq. (2) corresponds to the Standard Model coupling, while the tensors $T_{\mu\nu\lambda}^{(1)}$ and $T_{\mu\nu\lambda}^{(2)}$ give rise to *anomalous* TGCs. It may be noted that the dimension-4 tensor $T_{\mu\nu\lambda}^{(1)}$ can be absorbed in $T_{\mu\nu\lambda}^{(0)}$ with a coefficient $\kappa_\gamma = 1 + \Delta\kappa_\gamma$. However, in our work we have kept these tensors distinct as representing the SM and beyond-SM parts. Thus $\Delta\kappa_\gamma$ and λ_γ parametrize the strength of these beyond-SM contributions—which agrees with the common usage by most experimental collaborations.¹ It is reasonable to assume that $\Delta\kappa_\gamma$ will not be more than a few percent, for otherwise these corrections would have been detected when the W itself was discovered, or when its properties were precisely measured at the CERN LEP-2 [16] and the Fermilab Tevatron [17]. It is also traditional to parametrize the mass-suppression of the dimension-6 operator $T_{\mu\nu\lambda}^{(2)}$ with a factor M_W^{-2} . However, if the operator arises from new physics at a scale Λ , the corresponding coefficient should have been ξ/Λ^2 , where ξ is some coupling—perhaps $\mathcal{O}(1)$ —and hence, we can identify

$$\lambda_\gamma = \xi \left(\frac{M_W}{\Lambda} \right)^2. \quad (3)$$

In fact, setting $\xi = 1$, and $\Lambda = 1$ TeV, we get $\lambda_\gamma \simeq 0.0065$. We may thus expect λ_γ to lie an order of magnitude below $\Delta\kappa_\gamma$, and, in fact, we shall see below that this is indeed true for the experimental constraints.

We remark in passing that there are also CP -violating contributions to the $W^+W^-\gamma$ vertex, which can be parametrized in terms of two coupling constants $\tilde{\kappa}_\gamma$ and $\tilde{\lambda}_\gamma$. However, these are already constrained to be very small from the measurement of the electric dipole moment of the neutron [18], and hence we will not consider them further in this article. It is also possible—in fact, plausible—that if the photon has anomalous couplings with a W^+W^- pair, then the Z boson may also have such anomalous couplings,

¹Strictly speaking, there are SM contributions to $\Delta\kappa_\gamma$ and λ_γ at higher orders. For example, at the one-loop level, there could be contributions of the order of (few) $\times 10^{-4}$ at a center-of-mass energy of TeV strength [15]. These are negligible in the current experimental studies, which, to date, only put constraints at the level of 10^{-2} .

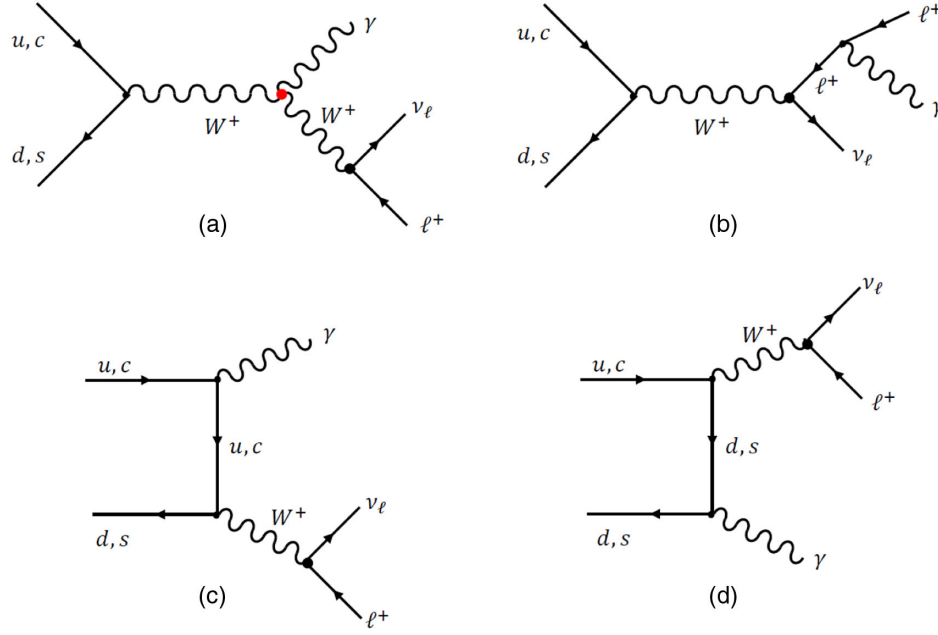


FIG. 1. Feynman diagrams contributing to the final state $\gamma\ell^+\nu_\ell$ at a hadron collider, with initial $u\bar{d}$ (or the more suppressed $c\bar{s}$) partonic states. These diagrams correspond to both the signal and the background, since the $W^+W^-\gamma$ vertex, indicated by the red dot in diagram (a), has both SM and anomalous contributions.

which may be related in some way by the gauge invariance of the SM [6]. However, the philosophy adopted in this article is that these will not affect the measurement in question and can, therefore, be kept outside the scope of the discussion. Experimental bounds involving WW production [16,19,20] have to consider this possibility and hence always carry a caveat about the choice of WWZ couplings.

The production of a W^\pm associated with a hard transverse photon is one of the most standard processes which one considers at a hadron collider [21,22]. It occurs through a pair of dissimilar quarks, e.g., u and d , as the initial-state partons, which are required for single W boson production. A photon can then be radiated off any of the internal or external legs of the corresponding diagram. However, if we allow the W^\pm to decay further into a charged lepton ℓ^\pm and the corresponding neutrino ν_ℓ , we will have one more diagram where a photon is radiated off the charged lepton. The final state consists, then, of a photon, a lepton and missing energy from the neutrino. One would also require a jet veto to keep the process hadronically quiet. The four diagrams at leading order are illustrated in Fig. 1.

When these diagrams are evaluated, the Feynman amplitude can be written

$$\mathcal{M}(\Delta\kappa_\gamma, \lambda_\gamma) = \mathcal{M}_{\text{SM}} + \Delta\kappa_\gamma \mathcal{M}_\kappa + \lambda_\gamma \mathcal{M}_\lambda \quad (4)$$

squaring which, it follows that the cross section will be a combination of terms

$$\begin{aligned} \sigma(\Delta\kappa_\gamma, \lambda_\gamma) &= \sigma_{\text{SM}} + (\Delta\kappa_\gamma)^2 \sigma_\kappa + \lambda_\gamma^2 \sigma_\lambda \\ &+ \Delta\kappa_\gamma \sigma_{\kappa,\text{SM}} + \lambda_\gamma \sigma_{\lambda,\text{SM}} + \Delta\kappa_\gamma \lambda_\gamma \sigma_{\kappa,\lambda} \quad (5) \end{aligned}$$

where the terms on the first line of Eq. (5) arise from the squares of the corresponding terms in Eq. (4), while the terms on the second line are the respective interference terms. Since $\Delta\kappa_\gamma$ and λ_γ are small, it is clear that σ_{SM} will be the dominant term—or dominant background—while the other terms in Eq. (5) will constitute a small signal. Of these, the terms linear in $\Delta\kappa_\gamma$ and λ_γ will generally be the largest. The challenge is, therefore, to isolate the extremely small signal from the large SM background by the judicious use of kinematic cuts and distributions. At this point, we note that QCD corrections to the $W\gamma$ process may increase [23] the overall cross section by 30%–40%. However, these may be expected to be rather similar for both signal and background, and hence they are not taken into account in our analysis.

In the experimental situation, our concern is with a hadronically quiet final state consisting of a hard transverse photon, a hard transverse lepton and substantial missing energy. This is a very clean signal and, barring issues like pileup and multiple interactions at the LHC, may be expected to constitute a strong probe for the underlying physics—in this case, the TGC concerned. Since the final state is so simple, there exists only a small number of kinematic variables which are invariant under longitudinal boosts, and these, together with the cuts we have imposed on them, are listed below.

- (A) The magnitude of the transverse momentum of the photon ($p_{T\gamma}$), which we require to satisfy $p_{T\gamma} \geq 60$ GeV.
- (B) The pseudorapidity of the photon (η_γ), which we require to satisfy $\eta_\gamma \leq 2.5$.
- (C) The magnitude of the transverse momentum of the lepton ($p_{T\ell}$), which we require to satisfy $p_{T\ell} \geq 40$ GeV.
- (D) The pseudorapidity of the lepton (η_ℓ), which we require to satisfy $\eta_\ell \leq 2.5$.
- (E) The magnitude of the missing transverse momentum (p_T), which we require to satisfy $p_T \geq 40$ GeV.
- (F) The so-called angular separation between photon and lepton ($\Delta R_{\gamma\ell}$), which we require to satisfy $\Delta R_{\gamma\ell} \geq 0.4$.

The cuts in (A)–(E) are driven more by ease of identification of the final state and the detector coverage, while (F) is included to suppress the collinear photons which are preferred by the SM diagram in Fig. 1(b).

In addition to the above, if we consider the vector momenta in the transverse plane, which we denote $\vec{p}_{T\gamma}$, $\vec{p}_{T\ell}$ and \vec{p}_T , we can construct three more variables which are invariant under longitudinal boosts. These are

$$\begin{aligned}\Delta\varphi_{\gamma\ell} &= \cos^{-1}\left(\frac{\vec{p}_{T\gamma} \cdot \vec{p}_{T\ell}}{p_{T\gamma}p_{T\ell}}\right) \\ \Delta\varphi_{\gamma p_T} &= \cos^{-1}\left(\frac{\vec{p}_{T\gamma} \cdot \vec{p}_T}{p_{T\gamma}p_T}\right) \\ \Delta\varphi_{\ell p_T} &= \cos^{-1}\left(\frac{\vec{p}_{T\ell} \cdot \vec{p}_T}{p_{T\ell}p_T}\right).\end{aligned}\quad (6)$$

These angular variables are known to be highly sensitive to momentum-dependent operators [9] and since the tensors $T_{\mu\nu\lambda}^{(1,2)}$ are of this kind, we may expect them to carry some signs of the anomalous TGCs. In fact, we find that the only variables which are sensitive to these are the transverse momenta in (A), (C) and (E) above, and these angular variables in Eq. (6).

Finally, to ensure good convergence of our Monte Carlo simulations, we construct [21,22] the variable M_{TW} , where

$$M_{TW}^2 = 2p_{T\ell}p_T(1 - \cos \Delta\varphi_{\ell p_T}) \quad (7)$$

and impose a cut $M_{TW} \geq 30$ GeV. The effect of these successive kinematic cuts on the terms in the cross section is shown in Table I. Any stronger cuts would result in severe loss in the TGC signal, both for $\Delta\kappa_\gamma$ and λ_γ .

If we consider the total cross section, as given above, the limits one can put on the parameters $\Delta\kappa_\gamma$ and λ_γ are already strong. The actual number of signal events (in thousands) expected are shown in the panels marked (a) and (b) in Fig. 2, assuming an integrated luminosity of 100 fb^{-1} . The abscissa in (a) and (b) shows, respectively, the values of $\Delta\kappa_\gamma$ and λ_γ , each assuming that the other is zero. The region

TABLE I. Cut flow table showing the effect of different kinematic cuts on the principal terms in the cross section. As may be expected, the SM contribution is brought down to about one tenth, whereas the others are reduced to roughly a third and a fifth respectively. The large value of σ_λ is due to the inappropriate choice of M_W^2 as the suppression factor—if we had chosen $\Lambda = 1$ TeV instead, these cross sections would be suppressed by a factor $(M_W/1 \text{ TeV})^2 \approx 6.4 \times 10^{-3}$, which would bring them on par with the previous columns.

Cut	σ_{SM}	σ_κ	σ_λ
$p_{T\gamma} \geq 60$ GeV	430.11 fb	737.82 fb	41.89 pb
$p_{T\gamma} \geq 60$ GeV	100.0%	100.0%	100.0%
$p_{T\ell} \geq 40$ GeV	70.25%	75.70%	85.55%
$p_T \geq 40$ GeV	22.82%	52.34%	70.77%
$M_{TW} \geq 30$ GeV	20.68%	43.13%	55.11%
$\eta_\gamma \leq 2.5$	15.89%	36.88%	53.50%
$\eta_\ell \leq 2.5$	12.28%	32.61%	52.24%
$\Delta R_{\gamma\ell} \geq 0.4$	11.30%	32.60%	52.26%
	48.57 fb	240.52 fb	21.89 pb

marked in grey corresponds to the 95% confidence level (C.L.) fluctuation in the SM prediction. Solid vertical lines indicate the current experimental bounds² from $W\gamma$ production at the LHC [21,22], which directly constrains the $WW\gamma$ vertex, whereas broken vertical lines indicate the bounds from WW production [19,20], where there are contributions from both $WW\gamma$ and WWZ vertices. As explained above, these constraints are not as solid as those obtained from $W\gamma$ production. However, it is immediately obvious that the signal considered in this work can achieve the 95% C.L. even at values which are comparable with the WW constraints, and certainly far smaller than the current $W\gamma$ constraints.

If the plots in the upper panels of Fig. 2 indicate strong constraints with a luminosity of 100 fb^{-1} , it is relevant to ask what may be achieved at the high-luminosity upgrade of the LHC (HL-LHC), where the integrated luminosity may go as high as 3 ab^{-1} . To determine the search limits, we can determine the signal significance $\chi^2(L, \Delta\kappa_\gamma, \lambda_\gamma)$ as a function of luminosity L as

$$\chi^2(L, \Delta\kappa_\gamma, \lambda_\gamma) = \left[\frac{L\{\sigma(\Delta\kappa_\gamma, \lambda_\gamma) - \sigma_{\text{SM}}\}}{\sqrt{L\sigma_{\text{SM}}}} \right]^2 \quad (8)$$

assuming Gaussian random fluctuations in the background $\delta(L\sigma_{\text{SM}}) = \sqrt{L\sigma_{\text{SM}}}$. For this study, we ignore systematic errors, or, more properly, assume that they will be small enough to be ignored, compared to the statistical error. Now if, for a given value of L , the value(s) of $\Delta\kappa_\gamma$ and/or λ_γ satisfy $\chi^2(L, \Delta\kappa_\gamma, \lambda_\gamma) > 1.96$, we qualify the signal for an anomalous

²The constraints from ATLAS [19,21] and CMS [20,22] are not obtained from the total cross section, but from a study of the p_T distributions of the final states. However, they are included here for purposes of comparison.

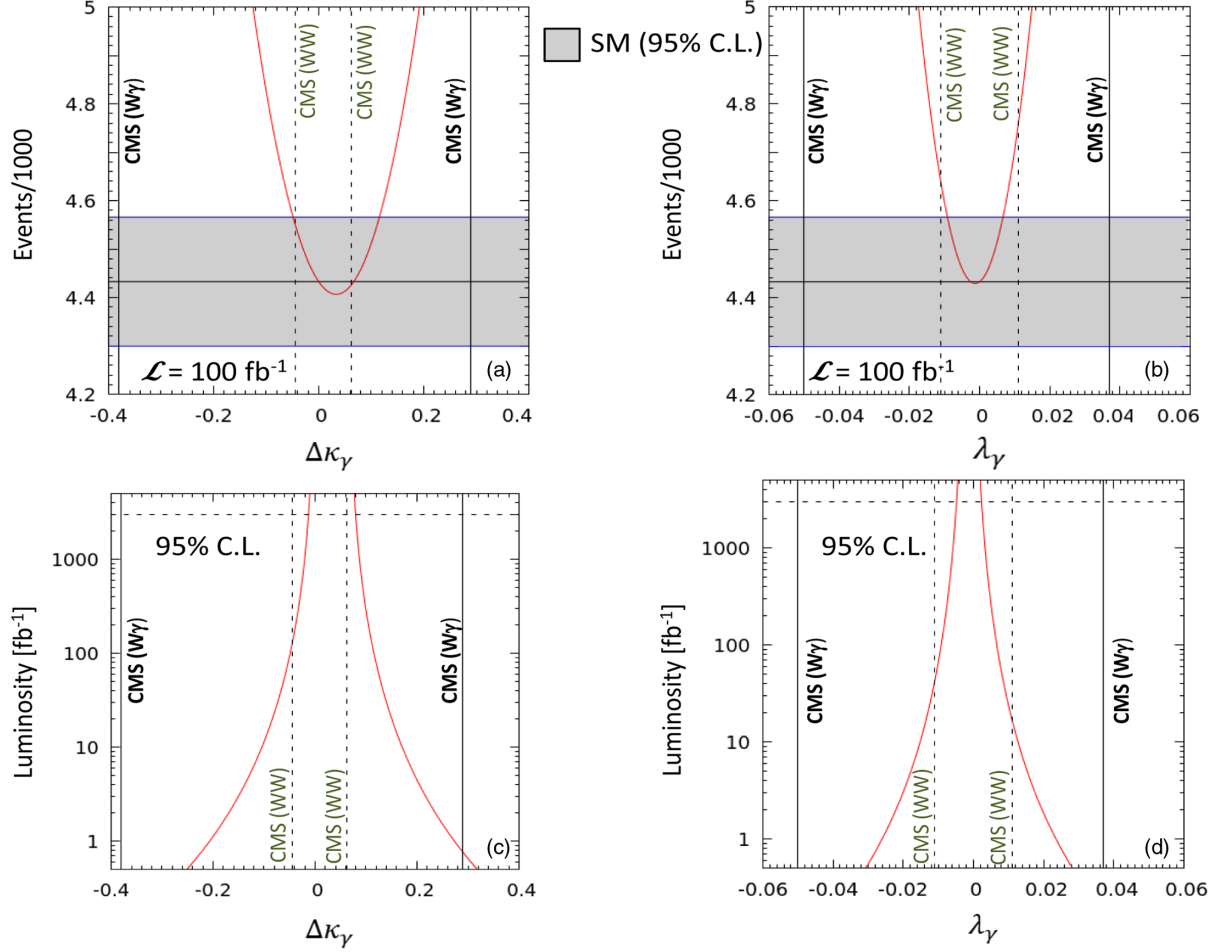


FIG. 2. Constraints on the anomalous $WW\gamma$ couplings from consideration of the total cross section, assuming an integrated luminosity of 100 fb^{-1} . The upper panels, marked (a) and (b), correspond to the variation in the excess in events per thousand over the SM prediction for the cases (a) $\Delta\kappa_\gamma \neq 0, \lambda_\gamma = 0$ and (b) $\Delta\kappa_\gamma = 0, \lambda_\gamma \neq 0$. The horizontal line shows the SM prediction and the shaded portion corresponds to its variation at 95% C.L. Solid vertical lines marked CMS($W\gamma$) correspond to the Run-1 CMS bounds on the corresponding anomalous coupling from $W\gamma$ production [22] and broken verticals marked CMS(WW) correspond to similar bounds obtained from WW production [20], assuming that $WW\gamma$ and WWZ anomalous couplings are related through $SU(2)$ symmetry. The lower panels, marked (c) and (d) respectively, show the corresponding 95% C.L. search limits (see text) when the luminosity is varied up to 5 ab^{-1} , with a horizontal broken line to indicate the machine limit of 3 ab^{-1} for the HL-LHC.

TGC as observable at 95% C.L. The corresponding variations, for the cases (c) $\Delta\kappa_\gamma \neq 0, \lambda_\gamma = 0$ and (d) $\Delta\kappa_\gamma = 0, \lambda_\gamma \neq 0$ are plotted in the lower panels of Fig. 2. It may immediately be seen that even with a very low integrated luminosity, the 13 TeV LHC does immensely better than the Run-1 data, and with an integrated luminosity of 1 ab^{-1} , the direct constraints which may be obtained from the total cross section are better than those even from WW production (which involve the WWZ couplings), except for one case $\Delta\kappa_\gamma > 0, \lambda_\gamma = 0$. At this juncture it is relevant to note the asymmetry of the curves in each panel about the zero point, which can be attributed to large interference terms between the anomalous $WW\gamma$ operators and the SM ones.

We now address the principal question for which this work was taken up, and that is whether the study of differential cross sections instead of the total cross section

can help better in identifying anomalous $WW\gamma$ couplings. We have made a careful study of practically all the straightforward kinematic variables it is possible to construct with a $\gamma\ell p_T$ final state. It turns out that the ones which are sensitive to the anomalous couplings, i.e., the ones for which the anomalous operators behave differently than the SM operators, are those listed below:

The effect of the anomalous TGCs on these is, of course, different for different observables, and this is illustrated in Figs. 3 and 4. In Fig. 3 we show three histograms in each panel, for the bin-wise quantity

$$N_{\text{excess}} = L \left(\frac{d\sigma}{dv_X} - \frac{d\sigma_{\text{SM}}}{dv_X} \right), \quad (9)$$

where L is the integrated luminosity and v_X is the corresponding variable in Table II. In each panel of

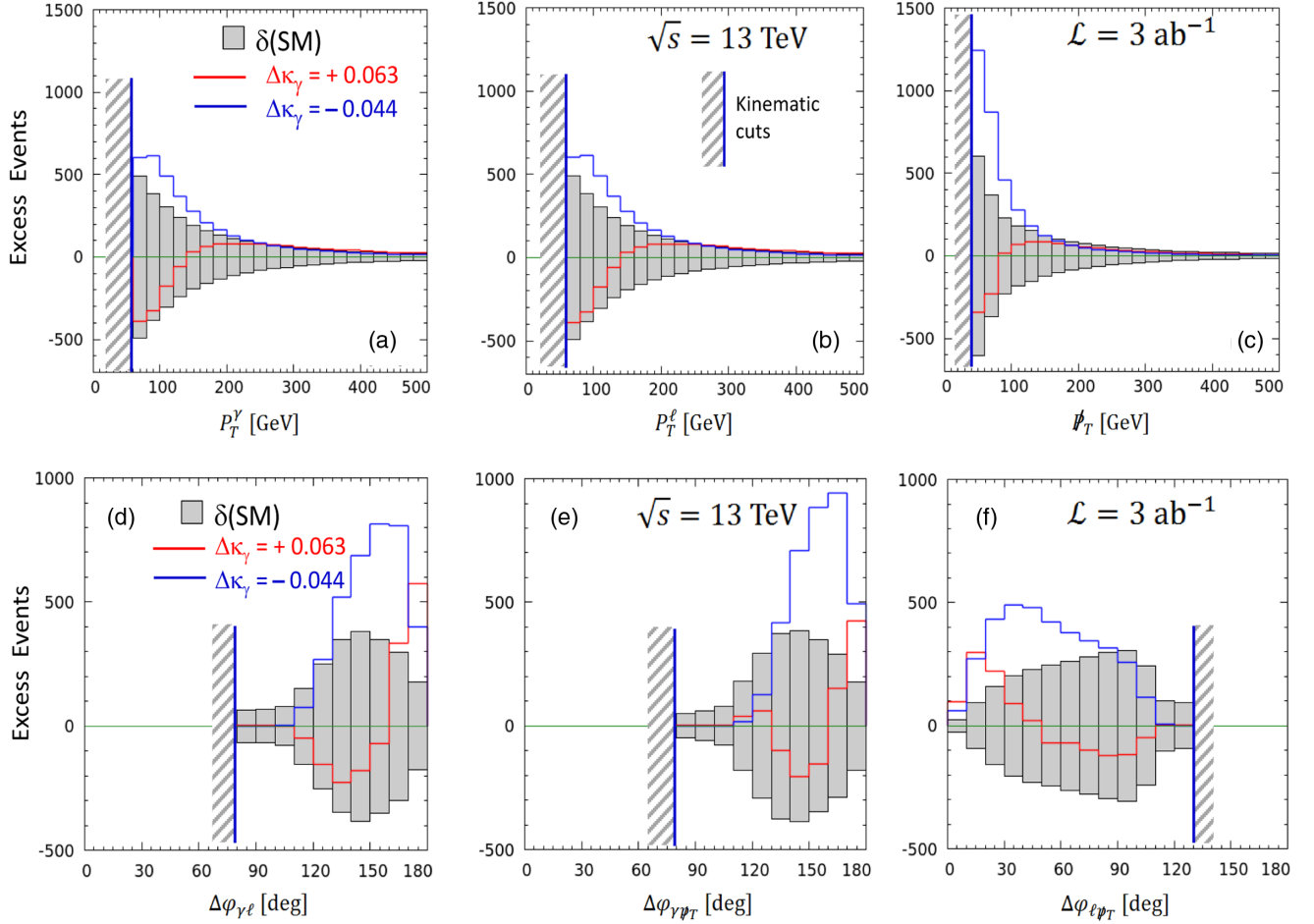


FIG. 3. Background-subtracted kinematic distributions for the different variables listed above in the case of $\Delta\kappa_\gamma \neq 0$ with $\lambda_\gamma = 0$. The panels are marked (a), (b), etc. according to the legend in the text. Red histograms correspond to the signal with a positive value (marked) of $\Delta\kappa_\gamma$ and blue histograms correspond to negative values of $\Delta\kappa_\gamma$, while the shaded histograms correspond to the 95% C.L. fluctuations in the SM background. Vertical lines with hatching indicate the kinematic cuts listed in the text.

Fig. 3, the red histogram corresponds to the excess events as per Eq. (9) for $\Delta\kappa_\gamma = +0.063$, i.e., the more stringent CMS upper limit arising from the WW cross section [20], and the blue histogram indicates the corresponding lower limit $\Delta\kappa_\gamma = -0.063$. The solid shaded region represents the 95% C.L. fluctuations in the SM prediction, denoted $\delta(\text{SM})$. In each case, the kinematic cuts listed in the text above are shown by a vertical line and hatching. For these plots, we have set $L = 3 \text{ ab}^{-1}$, i.e., the maximum envisaged value of the HL-LHC.

If we consider the case of $\Delta\kappa_\gamma > 0$, i.e., the red histograms in Fig. 3, we can see that the number of excess events is substantially above the SM fluctuation for a significant number of bins, especially as one goes towards higher magnitudes of p_T and for back-to-back vectors in the transverse plane, except for the opening angle in the transverse plane between the decay products of the W , which tend to be aligned for the signal. In fact, in some of the bins, the deviation is rather large. On the other hand, if we consider the case of $\Delta\kappa_\gamma < 0$, i.e., the blue histograms

in Fig. 3, the deviations are large only for really high magnitudes of p_T and even more extreme angles in the transverse plane than in the case of positive $\Delta\kappa_\gamma$.

Some of the salient features of the histograms in Fig. 3 are listed below.

- (i) In all the panels, the signal histograms for negative $\Delta\kappa_\gamma$ change sign over the selected range, whereas for positive $\Delta\kappa_\gamma$ they are monotone.
- (ii) Of the upper three panels, clearly the best signal will come from a study of the missing p_T , for, even for negative $\Delta\kappa_\gamma$, there are significant deviations over 100 GeV.
- (iii) In the lower three panels, all show large deviations from the SM background. It is not clear by inspection which of these three variables is best suited to find the signal. For this, we must develop a suitable numerical metric.

We then turn to the other anomalous coupling λ_γ , in the case when $\Delta\kappa_\gamma = 0$. This is illustrated in Fig. 4, where we show the same three histograms in each panel as for Fig. 3, for the

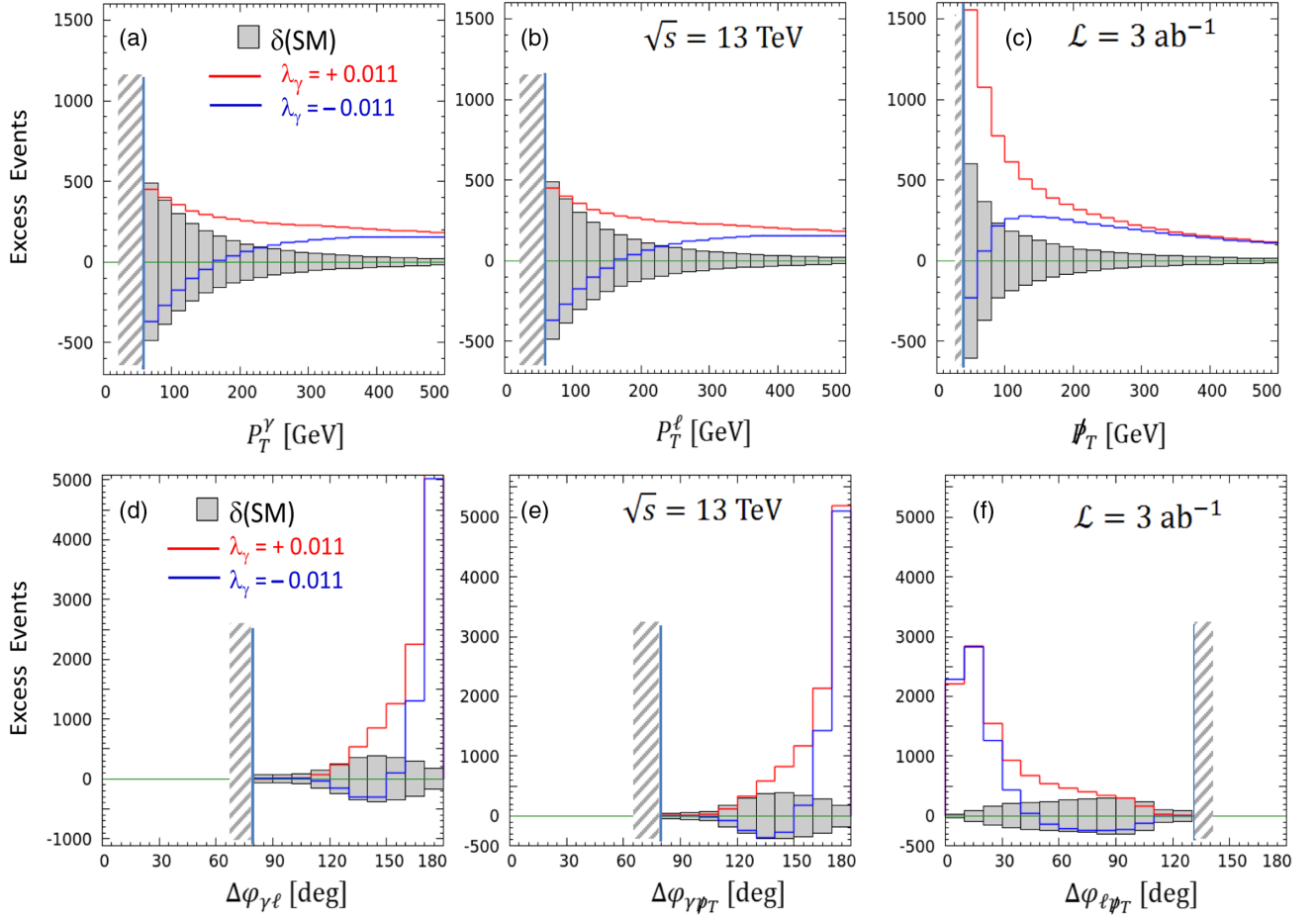


FIG. 4. Background-subtracted kinematic distributions for the different variables listed above in the case of $\lambda_\gamma \neq 0$ with $\Delta\kappa_\gamma = 0$. The panels are marked (a), (b), etc. according to the legend in the text. Red histograms correspond to the signal with a positive value (marked) of λ_γ and blue histograms correspond to negative values of λ_γ , while the shaded histograms correspond to the 95% C.L. fluctuations in the SM background. Vertical lines with hatching indicate the kinematic cuts listed in the text.

bin-wise quantities as defined in Eq. (9) and the table below it. The notations and conventions of Fig. 4 are therefore identical with those of Fig. 3. Obviously the range of values of λ_γ is smaller, but this is, as explained before, due to the artificial scaling with M_W instead of some higher scale. Thus, the red (blue) histograms correspond to $\lambda_\gamma = +0.011(-0.011)$, which are, as before, CMS limits from WW production [20]. There have been slight improvements in this recently [14] to upper bounds $\lambda_\gamma = +0.0080(-0.0076)$, but these hardly make perceptible changes in the figure. Qualitatively, the deviations are rather similar to those in Fig. 3, and one cannot tell, just by inspection, which of the parameters is preferable. Thus, if

indeed, a deviation in these distributions from the SM prediction is found, we will encounter a difficult *inverse problem*, i.e., separation of signals from $\Delta\kappa_\gamma$ from those for λ_γ . In the present article, however, we feel that it is premature to address this problem. Instead, we focus on whether it will be possible to extend the discovery reach of the LHC by considering these distributions, rather than the total cross section. The time to address this distinction will come when a deviation is actually found.

In order to see if a distribution has enough deviation from the SM prediction to be observable at, say, 95% C.L., we need to construct a suitable numerical metric. We choose a simple-minded extension of the one in Eq. (8), in the form

TABLE II. List of kinematic variables whose distributions are sensitive to anomalous TGCs.

$X =$	(a)	(b)	(c)	(d)	(e)	(f)
$v_X =$	$p_{T\gamma}$	$p_{T\ell}$	p_T	$\Delta\phi_{\gamma\ell}$	$\Delta\phi_{\gamma p_T}$	$\Delta\phi_{\ell p_T}$

$$\chi_X^2(L, \Delta\kappa_\gamma, \lambda_\gamma) = \sum_{n=1}^{N_X} \left(\frac{N_{\text{excess}}^{(n)}}{\sqrt{N_{\text{SM}}^{(n)}}} \right)^2 \quad (10)$$

where the index n runs over all the bins, and

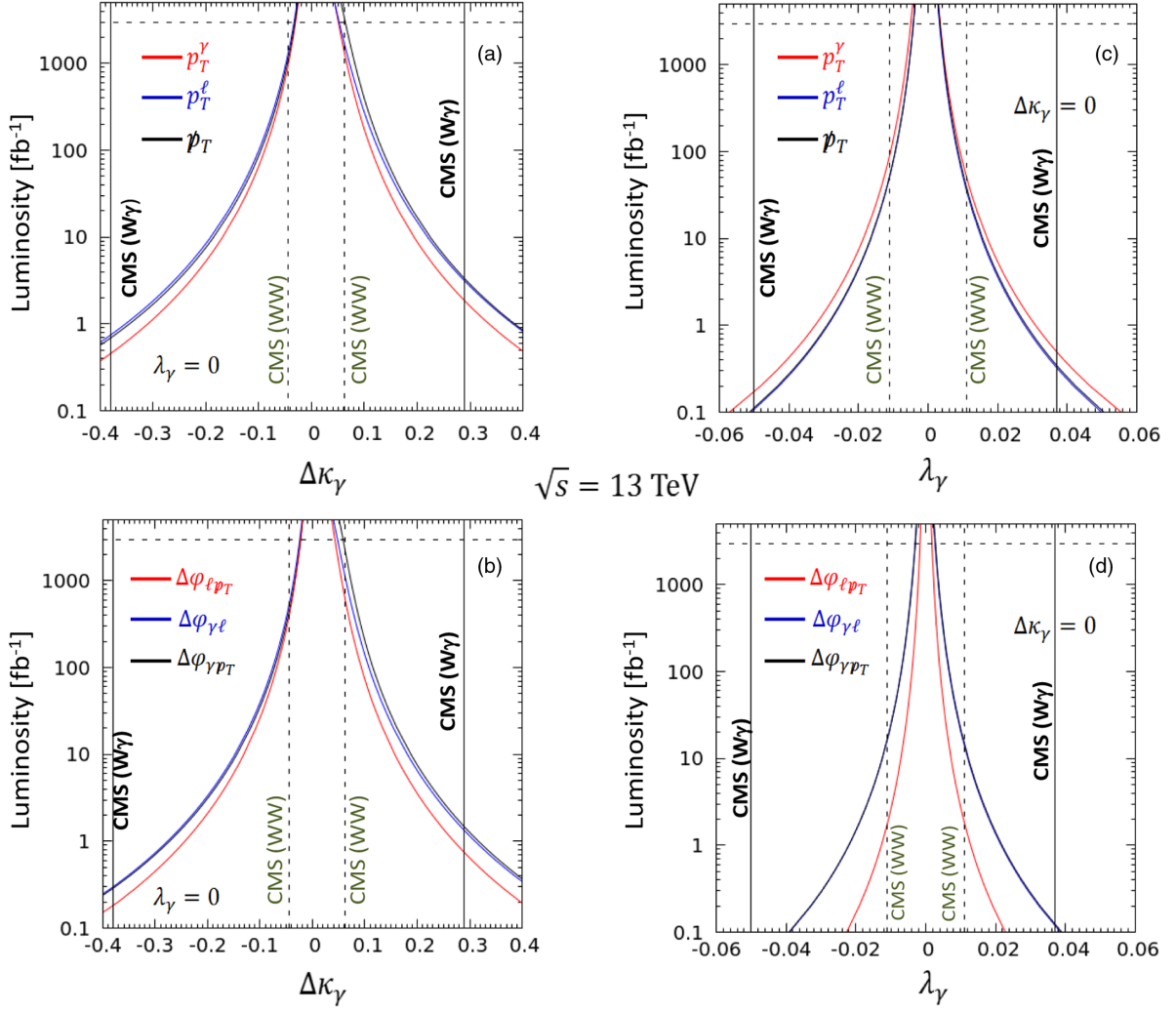


FIG. 5. 95% C.L. discovery limits for the case $\Delta\kappa_\gamma \neq 0$, $\lambda_\gamma = 0$ in the panels on the left, marked (a) and (b), and the case $\Delta\kappa_\gamma = 0$, $\lambda_\gamma \neq 0$ in the panels on the right, marked (c) and (d). Only three variables at a time have been shown in each panel to avoid clutter. The upper panels, marked (a) and (c), show the discovery limits for transverse momentum variables, while the lower panels, marked (b) and (d), show the discovery limits for azimuthal angle variables.

$$N_{\text{SM}}^{(n)} = L \frac{d\sigma_{\text{SM}}^{(n)}}{dv_X} \quad (11)$$

is the SM prediction in that bin. N_{excess} is defined in Eq. (9), but here it carries a bin index n , and L is, as usual, the integrated luminosity. The total number of bins N_X is not the same for all the different variables v_X , as a glance at Figs. 3 and 4 will show. We can now compare the calculated values of $\chi_X^2(L, \Delta\kappa_\gamma, \lambda_\gamma)$ with $\chi^2(N_X, 95\%)$ which is the probability that the SM cross section with N_X bins will undergo a 95% Gaussian fluctuation, faking a signal. If, for a given set of arguments, $\chi_X^2(L, \Delta\kappa_\gamma, \lambda_\gamma) > \chi^2(N_X, 95\%)$, we will assume the corresponding anomalous TGC to be discoverable at the LHC.

Our results for the different variables are shown in Fig. 5. The upper panels, marked (a) and (c), show the discovery limits for the transverse momentum variables p_T^γ , p_T^ℓ and p_T

in the two cases (a) $\Delta\kappa_\gamma \neq 0$, $\lambda_\gamma = 0$ and (c) $\Delta\kappa_\gamma = 0$, $\lambda_\gamma \neq 0$ respectively. Corresponding limits for the azimuthal angle variables $\Delta\varphi_{\gamma\ell}$, $\Delta\varphi_{\gamma p_T}$ and $\Delta\varphi_{\ell p_T}$ are similarly shown in the lower panels, marked (b) and (d) respectively. As before, the CMS limits from $W\gamma$ production [22], as well as those from WW production [20], are shown by solid and broken vertical lines respectively. As in Fig. 2, a broken horizontal line represents the maximum integrated luminosity envisaged at the HL-LHC, and therefore, its intersections with the different curves indicate the discovery limit of the machine.

If we now inspect the discovery limits in Fig. 5 and compare them with those in Fig. 2, the following conclusions emerge.

- (i) For $\Delta\kappa_\gamma < 0$, $\lambda_\gamma = 0$, the discovery limits from the total cross section are better than those from the distributions; among the distributions, the best constraints arise from $\Delta\varphi_{\ell p_T}$.

- (ii) For $\Delta\kappa_\gamma > 0$, $\lambda_\gamma = 0$, the discovery limits from the total cross section are no longer better; instead the p_T distributions are more efficient, especially as the luminosity increases above 100 fb^{-1} . The $\Delta\varphi_{\ell\nu_T}$ distribution can be used to get discovery limits comparable to those from the different p_T distributions, but not better.
- (iii) For $\Delta\kappa_\gamma = 0$, $\lambda_\gamma < 0$, the total cross section and the p_T distributions give similar discovery limits, while the discovery limits from the $\Delta\varphi_{\ell\nu_T}$ are significantly better and obviously improve as the integrated luminosity increases.
- (iv) For $\Delta\kappa_\gamma = 0$, $\lambda_\gamma > 0$, the total cross section gives better discovery limits than the p_T distributions, whereas the $\Delta\varphi_{\ell\nu_T}$ distribution always gives better sensitivity.

It is also interesting to note that of the three p_T distributions, the best results are obtained from different distributions in different regimes, whereas for the $\Delta\varphi$ distributions, $\Delta\varphi_{\ell\nu_T}$ is always the most sensitive. This sensitivity is likely to be due to interference between different helicity amplitudes [24], though that is not explicit in our calculations.

There is a very important lesson to learn from the above observations, viz., that there is no unique variable whose study will provide the maximum sensitivity to anomalous TGCs. A proper experimental study should, therefore, include *all* the variables considered above, including the total cross section. Currently, experimental results are mostly based on transverse momentum studies [16,21,22], but these, as our results indicate, are not always the most sensitive variables.

As all of the above results are considered at the leading order (LO) with a fixed set of parton distribution functions (PDFs), viz. the CTEQ-6L set, it is relevant to ask how robust these results are against QCD effects, such as scale variation, next-to-leading-order (NLO) effects and PDF uncertainties. One could also ask whether detector effects will lead to degeneration in the bounds obtainable from these variables. A complete analysis of these questions, we feel, is beyond the scope of the present work, and hence we have only made some preliminary studies in this regard.

To estimate these effects, as well as to validate our LO analyses, we have simulated the processes in questions using a combination of the following public domain software applications: MadGraph (version MG5-aMC-v2.4.2 [25]) to calculate cross sections, Pythia (version Pythia8219 [26]) for the simulation including fragmentation effects and Delphes (version Delphes-3.4.1 [27]) as a toy detector simulation. In this simulation, we trigger on a final state with a hard transverse photon and a hard transverse lepton, with a significant amount of missing p_T . In addition, we require our process to be hadronically quiet; i.e., we put a strong jet veto.

At the very outset, let us note that with the requirement of high- p_T , the detector effects, simulated by using the

Delphes package, with standard levels of smearing for the final-state photon and the lepton, are very small and may be safely neglected. The QCD effects are simulated by running the package MadGraph, which permit (i) the inclusion of NLO corrections; (ii) variation of the factorization scale Q , which we set to $M_W/2$, M_W and $2M_W$ to cover the expected range; and (iii) two PDF sets, the CTEQ-6 set [28] and the NNPDF-2.3 set [29]. Even though a large portion of these are removed by the jet veto and the hard p_T cuts, the residual effects are still not small, especially for the SM background where the change can be as much as a factor of 2. The new operators associated with the anomalous couplings $\Delta\kappa_\gamma$ and λ_γ are also changed, but by not much more than 20%–30% after application of the jet veto. However, our preliminary findings can be summarized as follows. Despite the smearing in distributions due to QCD effects, the variable $\Delta\varphi_{\ell\nu_T}$ remains the most sensitive of the azimuthal angle variables. We have, therefore, exhibited the normalized distributions in this variable in Fig. 6.

In Fig. 6, the black histograms correspond to the normalized SM distribution, with the thickness indicating the maximum spread due to the QCD effects mentioned above. In the panel on the left, marked (a), we also show the normalized distribution setting $\Delta\kappa_\gamma = +1$, $\lambda_\gamma = 0$ as a blue histogram with the same convention. In the panel on the right we also show the normalized distribution setting $\Delta\kappa_\gamma = 0$, $\lambda_\gamma = +1$ as a red histogram with the same convention. If we compare these with Figs. 3(f) and 4(f), it can be seen that despite some possible changes in the details, the qualitative features of the distributions are retained, which emboldens us to continue with the analysis in the same way as done for the leading-order calculation. However, it cannot be denied that all this does have an effect on the χ^2 . As mentioned above, a full study of the detailed effects for all the distributions is beyond the scope of this work, though it should certainly be taken up before the experimental data come in [30]. Instead, we exhibit our results for the χ^2 analysis using the $\Delta\varphi_{\ell\nu_T}$ variable in Fig. 7. In Fig. 7, we have plotted the graphs for integrated luminosity versus the minimum accessible values of (a) $\Delta\kappa_\gamma$ and (b) λ_γ respectively, taking into account the QCD effects in the distribution of $\Delta\varphi_{\ell\nu_T}$. The LO contributions, with $Q = M_W$, as used in all the other plots, are shown as solid red lines. The solid curves correspond to CTEQ-6 PDFs, and the dotted-dashed curves to NNPDF choices. Blue, black and green colors correspond to $Q = \frac{1}{2}M_W$, M_W and $2M_W$ respectively. The yellow-shaded region is the envelope of all these curves and may be taken as an indicator of the overall smearing due to QCD effects.

A glance at the QCD effects shows that they are clearly asymmetric, and hence arise principally from the interference terms. This is consistent with the maximum change happening in the SM contribution. For $\Delta\kappa_\gamma$, it leads to

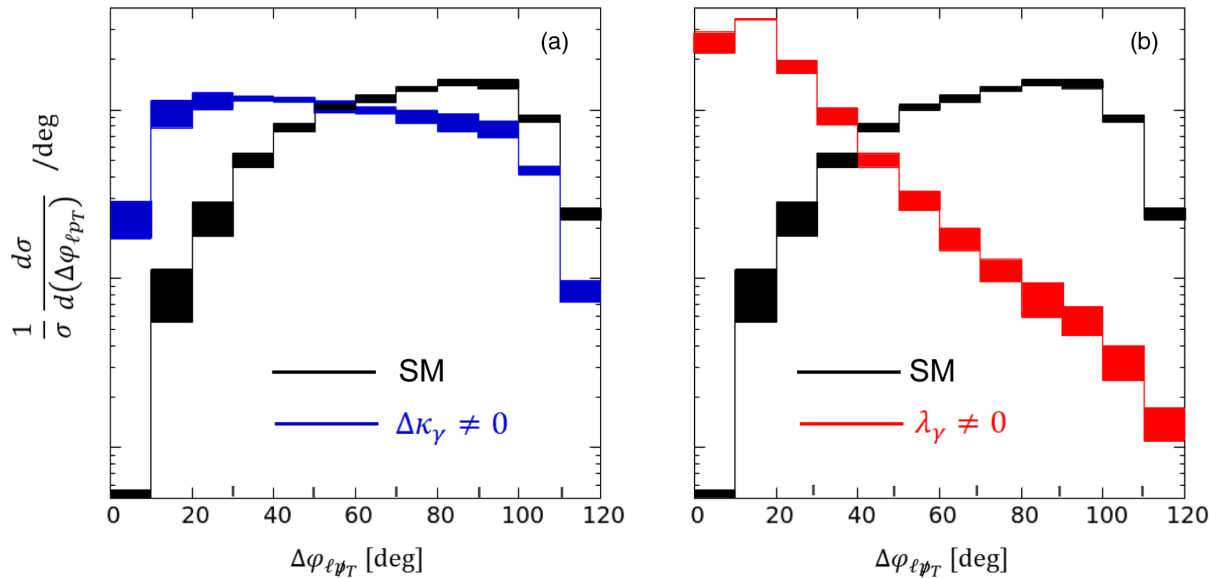


FIG. 6. QCD smearing of normalized distributions in $\Delta\varphi_{\ell\phi_T}$ for (a) the case $\Delta\kappa_\gamma \neq 0, \lambda_\gamma = 0$, and (b) the case $\Delta\kappa_\gamma = 0, \lambda_\gamma \neq 0$. In each case, the black histograms correspond to the SM distribution.

dilution of the LO results for negative $\Delta\kappa_\gamma$, but to a strengthening for positive $\Delta\kappa_\gamma$. On the other hand, for λ_γ , we have a strengthening (and very little spread) for negative λ_γ , but a large smearing as well as dilution for positive λ_γ . We may expect all the χ^2 analyses for different distributions to have such effects. This underlines the importance of considering all the variables, as mentioned above, before the potential of the LHC to probe anomalous TGCs is fully realized.

Thus far, we have only considered one of the TGCs at a time, viz., either $\Delta\kappa_\gamma \neq 0, \lambda_\gamma = 0$ or $\Delta\kappa_\gamma = 0, \lambda_\gamma \neq 0$. While convenient from a purely phenomenological standpoint, this is hard to justify from a top-down approach, for the same new physics which creates nonzero $\Delta\kappa_\gamma$ could very well generate nonzero λ_γ as well. We now turn, therefore, to the study of this more realistic case of joint variation of the two parameters. The formulas in Eqs. (8) and (10) are naturally geared to handle this joint variation, so all that is required is to numerically vary both the parameters and perform the same kind of analysis as we have described above.

Our results for joint variation are shown in Fig. 8. The left panel, marked (a), shows the discovery limits that can be obtained using the total cross section. The inaccessible region at the 13 TeV LHC, assuming an integrated luminosity of $10(1000) \text{ fb}^{-1}$, is shaded in pink (red). For comparison, on the same panel we give the constraints from LEP-2 (black) and from the CMS (blue) and ATLAS (green) collaborations at the LHC Run-1. In each case the inside of the ellipse is not accessible and the region outside is ruled out. It is immediately obvious that, as was the case with one parameter at a time, the total cross section is a reasonably sensitive probe of anomalous TGCs, and in fact,

even with 10 fb^{-1} of data, it is as sensitive as the use of the WW production data (modulo the WWZ caveat). Sensitivity improves dramatically for 1000 fb^{-1} luminosity, as the tiny red shaded region indicates. However—and here lies the rub—the inaccessible region is star shaped, with four arms which stretch to possible large values of one of the parameters at a time. It is easy to see why these arise, for the significance is based on a single parameter, viz., the total cross section, and there will always be regions where the contributions to this from $\Delta\kappa_\gamma$ cancel with those from λ_γ , making the signal small or vanishing. Thus, although the total cross section can be used to probe the anomalous TGCs quite efficiently, there remain these four narrow wedges of the parameter space which are inaccessible to the LHC.

The situation can be radically improved by using a distribution, rather than the total cross section, for it is almost inconceivable that the extra contributions from $\Delta\kappa_\gamma$ will undergo a bin-by-bin cancellation with those from λ_γ , given that the distributions are somewhat different, as shown in Figs. 3 and 4. To be precise, the same pair of values which cause cancellation of anomalous effects in one bin may not cause cancellation in another bin, and hence, the overall value of χ^2 will not be rendered small. This is illustrated in the right panel, marked (b), of Fig. 8, where we use the distribution in $\Delta\varphi_{\ell\phi_T}$ to obtain 95% C.L. discovery limits. Here, corresponding to different values of the integrated luminosity, we show the discovery limits as elliptic regions in the same way as the experimental collaborations. As usual, the interior of each ellipse is inaccessible to the LHC with the luminosity in question. The experimental constraints are given exactly as in the left panel, marked (a). It hardly needs to be mentioned that at

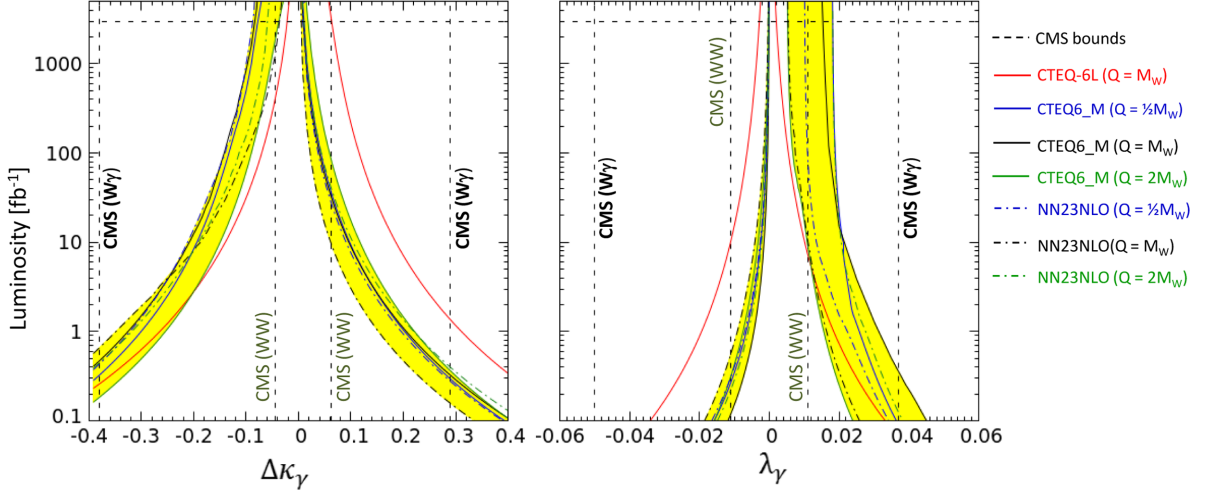


FIG. 7. QCD smearing of 95% C.L. discovery limits for the case $\Delta\kappa_\gamma \neq 0$, $\lambda_\gamma = 0$ in the panel on the left, marked (a), and the case $\Delta\kappa_\gamma = 0$, $\lambda_\gamma \neq 0$ in the panel on the right, marked (b). Only the variable $\Delta\varphi_{\ell p_T}$ has been considered. Solid (dotted-dashed) lines correspond to CTEQ-6 and NNPDF-2.3 parton densities and the color scheme is as follows: red for LO and blue, black and green for NLO with $Q = \frac{1}{2}M_W$, M_W and $2M_W$ respectively. The region shaded yellow is the envelope of the different QCD uncertainties. As in the previous figures, dashed lines indicate the CMS constraints.

the HL-LHC, very stringent constraints indeed could be obtained in case no deviation from the SM is seen. It may be noted, however, that even with this accuracy of measurement, the one-loop SM effects will not be accessible, though effects from new physics, such as the minimal supersymmetric Standard Model (MSSM), may be [15]. The above results will also be both strengthened and diluted by QCD effects, as shown for the single-parameter analyses above. We may thus expect the ellipses in Fig. 8 to get

distorted (though retaining their ellipticity) and smeared out on the same pattern as the curves in Fig. 7.

To summarize, then, we have considered the process $pp \rightarrow \gamma W^* \rightarrow \gamma \ell p_T$ at the 13 TeV run of the LHC, and studied possible implications of having anomalous (CP -conserving) $WW\gamma$ vertices in the theory. The choice of this process (which has a lower cross section than, say, W^+W^- pair production) is because the tagging of a final-state photon ensures that there is no contamination of the

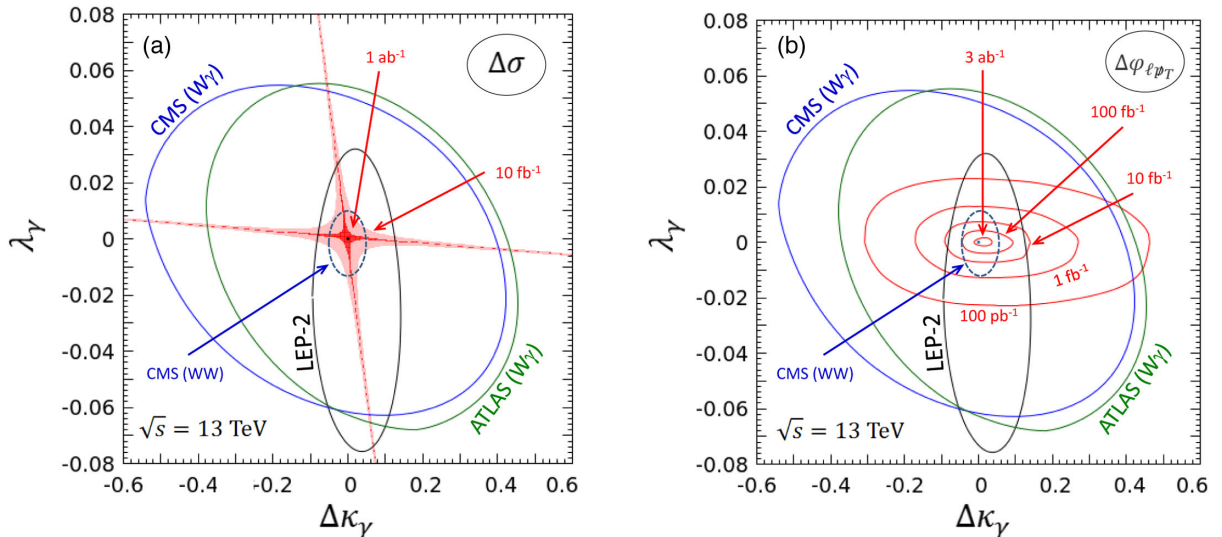


FIG. 8. Joint discovery limits at 95% C.L. on the anomalous couplings $\Delta\kappa_\gamma$ and λ_γ . The measurables used are (a) the total cross section and (b) the azimuthal angle variable $\Delta\varphi_{\ell p_T}$ respectively. In the left panel, marked (a), the regions shaded pink (red) are inaccessible to the LHC with 10(1000) fb^{-1} of integrated luminosity. Similar inaccessible regions lie inside the oblate ellipses (in red) on the right panel, marked (b). Experimental constraints from LEP-2 and from Run-1 of the LHC are shown as prolate ellipses in both panels. The tiny black dot at the center is, of course, the SM prediction at tree level.

new physics contribution with possible anomalous effects in the $WW\gamma$ vertex. We have shown that the anomalous $WW\gamma$ couplings may be constrained by considering not one, but seven independent observables, viz. the total cross section, three different p_T distributions and three different azimuthal angle variables. The relative efficacy of each of these has been studied in detail, making certain simplifying assumptions, such as the absence of initial-state/final-state radiation, pileup effects, systematic errors and detector effects. The first two we expect to be essentially eliminated by the rather severe kinematics cuts chosen for our analysis, but the latter ones can only be estimated by a thorough experimental analysis, which is beyond the scope of this work. Similarly, we have assumed that the kinematic cuts suggested by us will be effective at controlling backgrounds from $W + \text{jet}$ events (with a jet faking a photon). Under these assumptions, we have shown that the judicious use of the variables studied, especially the azimuthal angle variable $\Delta\varphi_{\ell p_T}$, can be used to pinpoint anomalous effects in the process in question, to a great degree of accuracy, as

the statistics collected by the LHC (and its HL upgrade) grow larger. QCD effects will cause some dilution or strengthening of these results, depending on the values of the TGCs, but the overall pattern will not change too radically. Such measurements would eventually probe not just large electroweak corrections in the TGC sector, but could also effectively constrain new physics involving modifications and mixings in the gauge sector. Of course, the most exciting scenario would be to see an unambiguous deviation from the SM prediction in any of the variables (or more than one variable) in the upcoming runs of the LHC, and it is on this hopeful note that we conclude this article.

ACKNOWLEDGEMENTS

The authors are grateful to Monoranjan Guchait, Sandhya Jain and Gobinda Majumder (CMS Collaboration) for discussions. They also thank an anonymous reviewer of this paper for pointing out the importance of QCD-based uncertainties in this analysis.

-
- [1] G. Aad *et al.* (ATLAS Collaboration), *Phys. Lett. B* **716**, 1 (2012); S. Chatrchyan *et al.* (CMS Collaboration), *Phys. Lett. B* **716**, 30 (2012).
- [2] ATLAS Collaboration, Summary plot for SUSY, https://atlas.web.cern.ch/Atlas/GROUPS/PHYSICS/CombinedSummaryPlots/SUSY/ATLAS_SUSY_Summary/ATLAS_SUSY_Summary.png; Summary plot for exotics, https://atlas.web.cern.ch/Atlas/GROUPS/PHYSICS/CombinedSummaryPlots/EXOTICS/ATLAS_Exotics_Summary/ATLAS_Exotics_Summary.png; CMS combined summary plot, https://twiki.cern.ch/twiki/pub/CMSPublic/PhysicsResultsCombined/exo-limits_ICHEP_2016.001.png.
- [3] J. L. Hewett, Theory summary, *53rd Recontres de Moriond, La Thuile, Italy* (2018), https://indico.in2p3.fr/event/16579/contributions/60906/attachments/47364/59542/Theory_Summary_Moriond_2018.pdf.
- [4] See, for example, J. Ellis, *Phil. Trans. R. Soc. A* **370**, 818 (2012).
- [5] W. Büchmüller and D. Wyler, *Nucl. Phys.* **B268**, 621 (1986); for a more recent review, see S. Dawson, [arXiv:1712.07232](https://arxiv.org/abs/1712.07232).
- [6] K. Hagiwara, R. D. Peccei, D. Zeppenfeld, and K. Hikasa, *Nucl. Phys.* **B282**, 253 (1987).
- [7] K. Hagiwara, S. Ishihara, R. Szalapski, and D. Zeppenfeld, *Phys. Lett. B* **283**, 353 (1992).
- [8] U. Baur and D. Zeppenfeld, *Phys. Lett. B* **201**, 383 (1988).
- [9] S. S. Biswal, R. M. Godbole, B. Mellado, and S. Raychaudhuri, *Phys. Rev. Lett.* **109**, 261801 (2012); S. S. Biswal, M. Patra, and S. Raychaudhuri, [arXiv:1405.6056](https://arxiv.org/abs/1405.6056); A. Azatov, J. Elias-Miro, Y. Reyimuaji, and E. Venturini, *J. High Energy Phys.* **10** (2017) 027; R. Li, X. M. Shen, K. Wang, T. Xu, L. Zhang, and G. Zhu, *Phys. Rev. D* **97**, 075043 (2018).
- [10] G. Buchalla, O. Cata, R. Rahn, and M. Schlaffer, *Eur. Phys. J. C* **73**, 2589 (2013); L. Bian, J. Shu, and Y. Zhang, *J. High Energy Phys.* **09** (2015) 206; A. Rosca, *Nucl. Part. Phys. Proc.* **273–275**, 2226 (2016); J. D. Wells and Z. Zhang, *Phys. Rev. D* **93**, 034001 (2016); S. M. Etesami, S. Khatibi, and M. Mohammadi Najafabadi, *Eur. Phys. J. C* **76**, 533 (2016); R. Rahaman and R. K. Singh, [arXiv:1711.04551](https://arxiv.org/abs/1711.04551); A. Falkowski, M. González-Alonso, A. Greljo, D. Marzocca, and M. Son, *J. High Energy Phys.* **02** (2017) 115; Z. Zhang, *Phys. Rev. Lett.* **118**, 011803 (2017).
- [11] T. Corbett, O. J. P. Éboli, J. Gonzalez-Fraile, and M. C. Gonzalez-Garcia, *Phys. Rev. Lett.* **111**, 011801 (2013); A. Butter, O. J. P. Éboli, J. Gonzalez-Fraile, M. C. Gonzalez-Garcia, T. Plehn, and M. Rauch, *J. High Energy Phys.* **07** (2016) 152.
- [12] D. R. Green, P. Meade, and M. A. Pleier, *Rev. Mod. Phys.* **89**, 035008 (2017).
- [13] C. Degrande, N. Greiner, W. Kilian, O. Mattelaer, H. Mebane, T. Stelzer, S. Willenbrock, and C. Zhang, *Ann. Phys. (Amsterdam)* **335**, 21 (2013).
- [14] A. M. Sirunyan *et al.* (CMS Collaboration), *J. High Energy Phys.* **04** (2019) 122.
- [15] G. Gounaris *et al.*, [arXiv:hep-ph/9601233](https://arxiv.org/abs/hep-ph/9601233).
- [16] See, for example, S. Schael *et al.* (ALEPH, DELPHI, L3, OPAL, and LEP Electroweak Collaborations), *Phys. Rep.* **532**, 119 (2013).
- [17] See, for example, C. E. Gerber *et al.* (TeV4LHC-Top Collaboration and Electroweak Working Group), [arXiv:0705.3251](https://arxiv.org/abs/0705.3251).

- [18] F. Boudjema, K. Hagiwara, C. Hamzaoui, and K. Numata, *Phys. Rev. D* **43**, 2223 (1991); D. Choudhury, J. Kalinowski, and A. Kulesza, *Phys. Lett. B* **457**, 193 (1999).
- [19] M. Aaboud *et al.* (ATLAS Collaboration), *Eur. Phys. J. C* **77**, 563 (2017).
- [20] A. M. Sirunyan *et al.* (CMS Collaboration), *Phys. Lett. B* **772**, 21 (2017).
- [21] G. Aad *et al.* (ATLAS Collaboration), *Phys. Rev. D* **87**, 112003 (2013); **91**, 119901(E) (2015).
- [22] S. Chatrchyan *et al.* (CMS Collaboration), *Phys. Lett. B* **701**, 535 (2011); *Phys. Rev. D* **89**, 092005 (2014).
- [23] J. Ohnemus, *Phys. Rev. D* **47**, 940 (1993); A. Denner, S. Dittmaier, M. Hecht, and C. Pasold, *J. High Energy Phys.* **04** (2015) 018.
- [24] G. Panico, F. Riva, and A. Wulzer, *Phys. Lett. B* **776**, 473 (2018).
- [25] J. Alwall, M. Herquet, F. Maltoni, O. Mattelaer, and T. Stelzer, *J. High Energy Phys.* **06** (2011) 128.
- [26] T. Sjöstrand, S. Mrenna, and P. Skands, *J. High Energy Phys.* **05** (2006) 026; *Comput. Phys. Commun.* **178**, 852 (2008).
- [27] J. de Favereau, C. Delaere, P. Demin, A. Giammanco, V. Lemaître, A. Mertens, and M. Selvaggi (DELPHES 3 Collaboration), *J. High Energy Phys.* **02** (2014) 057.
- [28] J. Pumplin, D. R. Stump, J. Huston, H.-L. Lai, P. Nadolsky, and W.-K. Tung, *J. High Energy Phys.* **07** (2002) 012.
- [29] R. D. Ball *et al.*, *Nucl. Phys.* **B867**, 244 (2013).
- [30] T. Bandyopadhyay, D. Bhatia, and S. Raychaudhuri (to be published).